Van-Thuyet Ngo

EFFECT OF SHAPE FACTOR ON THE HORIZONTAL RESPONSE OF PROTOTYPE UNBONDED FIBER REINFORCED ELASTOMERIC ISOLATORS UNDER CYCLIC LOADING

UTICAJ FAKTORA OBLIKA NA HORIZONTALNU REAKCIJU CIKLIČNOG OPTEREĆENJA PROTOTIPA ELASTOMERNOG IZOLATORA OJAČANOG NEVEZANIM VLAKNIMA

Originalni naučni rad / Original scientific paper
UDK /UDC:

Rad primljen / Paper received: 15.06.2020

Adresa autora / Author's address:
Faculty of Civil Engineering, Thuyloi University, 175 Tay Son, Dong Da, Hanoi, Vietnam email: thuyet.kcct@tlu.edu.vn

Keywords
- base isolation
- unbonded fiber reinforced elastomeric isolator
- shape factor
- rollover deformation
- horizontal response

Abstract

Unbonded fiber reinforced elastomeric isolator (U-FREI) is a device for improved seismic performance of low-rise buildings. Fiber layers are used as reinforcement to replace steel shims, as are normally used in conventional steel reinforced elastomeric isolator (SREI). Further, heavy steel-end-plates are not provided in U-FREI and this device is installed at the interface of foundation and superstructure without any connection. Shape factor (S), which is defined as the ratio of the loaded area to load-free area of an elastomer layer, is likely to have influence on the force-displacement behaviour of U-FREI. Most existing studies on U-FREIs are limited to low shape factors for scaled specimens (S < 10). In this study, effect of shape factor on the horizontal response of prototype U-FREIs (S > 10) under the vertical pressure and cyclic horizontal displacement simultaneously is investigated by both experiments and finite element (FE) analysis. It is observed that the effective horizontal stiffness of U-FREI with smaller shape factor is smaller than that of U-FREI with larger shape factor at any given amplitude of displacement. Further, peak values of compressive stress in elastomer layers of U-FREI with smaller shape factor are higher than those of U-FREI with larger shape factor, while peak values of shear strain in elastomer layers of these U-FREIs are quite comparable at any given applied displacement.

Ključne reči
- izolacija osnove
- elastomerni izolator ojačan nevezanim vlaknima
- faktor oblika
- deformacija valjanjem
- horizontalna reakcija

Izvod

Elastomerni izolator ojačan nevezanim vlaknima (U-FREI) se koristi za poboljšanje ponašanja niskih zgrada pri seizmičkom opterećenju. Slojevi vlakana se koriste kao ojačanje umesto uobičajenih čelično ojačanih elastomera (SREI). Pored toga, U-FREI ne sadrži teške čelične ploče, i instalira se na kontaktu između temelja i superstrukture bez ikakvih veza. Faktor oblika (S), koji se definiše kao odnos opterećene i neopterećene površine sloja elastomera, najverovatnije ima uticaja na izgled krive sila-pomeranje za U-FREI. Većina sadašnjih istraživanja vezanih za U-FREI su ograničena na niske vrednosti ovog faktora za modelirane uzorke (S < 10). U ovom radu se uzima u obzir uticaj faktora oblika na horizontalnu reakciju prototipa od U-FREI (S > 10) pod vertikalnim pritiskom i cikličnom horizontalnom pomeranju, a koji je ispitan eksperimentalno i analiziran metodom konačnih elemenata (FE). Uočeno je da je efektivna horizontalna krutost U-FREI elemenata sa manjim faktorom oblika niža u odnosu na one sa većim faktorom, bez obzira na amplitudu pomeranja. Štaviše, ekstremne vrednosti pritisnih napona u slojevima U-FREI elastomera sa nižim faktorom oblika su veće u poređenju sa U-FREI elastomerima sa većim faktorom oblika, dok su ekstremne vrednosti smičućih deformacija u oba slučaja slične bez obzira na primenjenu amplitudu pomeranja.

INTRODUCTION

Base isolation has been a popular means of seismic protection of structures. Its main concept is that structures are decoupled from the ground by introducing a layer of rubber bearings, friction bearings, springs, etc. between the superstructure and the substructure. The aim of seismic base isolation is mainly to avoid the transmission of seismic energy and forces from the ground or the substructure to the superstructure, and generally falls under the scope of passive structural vibration control technologies. Effectively, a seismic base-isolated structure has eigenperiods significantly larger than the eigenperiods of its conventional counterpart, and this inhibits the seismic energy transmission.

Among the various techniques of seismic base isolation, conventional steel reinforced elastomeric isolators (SREIs) have become one of the most widely accepted over the past decades. In these isolators, thin steel sheets are placed between rubber layers. The former are used as the reinforcing material, the purpose of which is to provide the necessary vertical stiffness to the isolator for taking the vertical forces of the superstructure. There are many types of SREIs, e.g., natural rubber bearing, high-damping rubber bearing and lead rubber bearing. In general, SREIs are used in highway bridges, large and/or important buildings in developed countries, e.g. Lou et al. /1/ presented the eigenvalue modal analyses of quasi-isolated highway bridges supported on SREIs in Illinois, USA; Shiravand and Rasouli /2/ carried out the effects of substructure mass participation on natural period of multi-column base isolated bridges; a seismic reliability of steel moment-resisting frame structures isolated by lead-rubber bearing systems was evaluated through an extensive parametric study /3/, etc. However, in more common structures, such as low-rise buildings they are not so widely used, partially due to high material, manufacturing, installation costs and also due to restrictions imposed by the various seismic codes worldwide. Some disadvantages of SREIs that limit their application to ordinary low-rise housing are their increased weight and the need of complicated and expensive processes for their construction (e.g. placement of thick end plates at the ends of the isolators, placing of the steel shims between the various rubber layers, etc.). Replacing the steel reinforcement with fiber reinforcement seems a good alternative, which leads to the construction of fiber reinforced elastomeric isolators (FREIs) /4/. Further improvements to FREIs are the unbonded FREIs (U-FREIs), which do not require a bonded or fastened connection between the substructure and the superstructure. Instead, they can be installed directly in the structure without any connection at their boundaries. It is evident that the U-FREIs are expected to reduce the construction costs, while their installation will become easier due to their low weight. Furthermore, due to the absence of steel boundaries for their connection to the sub- and superstructure, their size can be easily adjusted to satisfy design and geometry limitations on a case-by-case basis. Therefore, U-FREIs seem to be an attractive option for seismic mitigation of low-rise buildings in the developing countries like India, Nepal, Bangladesh, Indonesia, etc. Apart from the above, U-FREIs have higher energy dissipation than their bonded FREI counterparts, which gives them an additional advantage regarding seismic protection.

Various studies have been conducted with the purpose of evaluating the mechanical properties of the FREIs. Kelly and Takhirov /5-6/ studied the mechanical response of unbonded circular FREI and rectangular long-strip FREI and they concluded that it should be possible to produce a fiber-reinforced isolator that is significantly lighter that matches the behaviour of a steel-reinforced isolator. Moon et al. /7/ analysed experimentally seismic isolators reinforced with four types of fibers, i.e. carbon, glass, nylon and polyester. They found that the FREI reinforced by carbon gives higher vertical stiffness and superior to effective damping than that of SREI. Toopchi-Nezhad et al. /8-10/ conducted an experimental study on square carbon FREIs, from which they found that stable rollover response is a unique characteristic of U-FREIs which decreases the effective lateral stiffness of the bearings and optimizes their efficiency as seismic isolation devices. Also, the lateral response of U-FREIs was shown to be comparable to that of conventional high-damped SREIs. Russo and Pauletta /11/ carried out tests to investigate the effect of compressive stress, rubber typology, concrete roughness, aging and loading rate on elastomeric isolators reinforced by bi-directional carbon fiber fabrics (U-FREIs) on the friction behaviour of the latter whereas, Spizzuoco et al. /12/ investigated the seismic performance of square U-FREIs with recycled rubber under seismic loading both experimentally and with the FE method. All bearings deformed due to rollover, stemming from the unbounded boundary condition at their contact surfaces. After a series of cyclic loading tests on SREIs, FREIs and U-FREIs, in which the effect of vertical stress, horizontal deflection, bearing height, number of elastomer and reinforcement layers, reinforcement material, and type of bearing support on the effective shear modulus and damping coefficient was studied. Strauss et al. /13/ provided suggestions for improved design guidelines about reinforced elastomeric bearings. Dezfuli and Alam /14/ examined the operation of carbon FREIs under various loading conditions. They concluded that the bearings perform well up to 100% shear strain, although there may be partial delamination between rubber and the steel supporting plates, and that the percentages of fiber reinforced and elastomeric layers inside the bearing in terms of thickness determine its stiffness and energy dissipation capacity. Van Engelen et al. /15/ presented an additional parameter that can optimize the design of U-FREIs, namely the presence of holes inside an isolator. They performed an experimental study on the horizontal and vertical response of square and strip U-FREIs, showing a favourable decrease in horizontal stiffness accompanied by an increase in energy dissipation capacity. Toopchi-Nezhad /16/ proposed two simplified analytical models for the evaluation of the horizontal stiffness of U-FREIs that show good agreement with available experimental and numerical results. The effect of the direction at which the horizontal load is applied with reference to square FREIs and U-FREIs on the performance of the latter were examined /17/. It was found that U-FREIs are more effective than bonded FREIs and also the developed stresses are significantly lower in U-FREIs. Ngo et al. /18/ evaluated the horizontal response of prototype FREIs and U-FREIs under horizontal cyclic loading. Similar to /15/, they found that the rollover deformation reduces the effective horizontal stiffness and increases the equivalent viscous damping. In a subsequent study, Ngo et al. /19-20/ presented the effect of shear modulus and horizontal loading direction on the performance of square U-FREIs. Losanno et al. /21/ carried out the bidirectional shaking table tests of unbonded recycled rubber fiber-reinforced bearings. An effort to apply the recycled rubber fiber-reinforced bearings for residential buildings in developing countries was conducted, /22/.

The aforementioned description has highlighted the various parameters affecting the response of U-FREIs (i.e. material properties, configuration, loading direction, friction between the isolator and the supporting areas, etc.). In addition to these, it has been generally known that the shape factor of an isolator affects its mechanical properties (vertical, horizontal and bending stiffness). The shape factor (S) is defined as the ratio of the loaded area to the load-free area of an elastomeric layer /23/. While the effect of shape factor on vertical stiffness and effective bending stiffness of U-FREIs can be described through simple formulas, the effect on effective horizontal stiffness is more complicated, due to the presence of rollover response. The latter effect has not been adequately addressed in the literature. In addition, the shape factors considered in most studies takes values lower or equal to 10. Therefore, there is not much information for isolators with shape factors ranging from 10 to 20, which are typical for seismic isolation /23/. In addition, most previous studies are considered for scaled elastomeric isolators with different thickness of elastomer layer, reinforcement layer and thus different total height of isolators, and different material properties. Thus, a holistic study involving prototype U-FREIs with the same material properties, same thickness of elastomer as well as reinforcement layers and same total height but with different shape factors is required to evaluate the influence of shape factor on their behaviour.

In this study the horizontal response of prototype U-FREIs under cyclic loading is investigated. Both, experimental tests as well as numerical simulations are used for the evaluation of the response. Regarding the experimental study, four specimens are tested for estimating their horizontal stiffness, energy dissipation capacity and equivalent viscous damping. Two different sizes of 250×250×100 mm and 310×310×100 mm with shape factors of 12.5 and 15.5, respectively, are considered. Furthermore, finite element models of the U-FREIs considered in this study are developed and verified by experimental results. The FE models are used for the prediction of the isolator response for displacements higher than those of the experimental tests, and also for the assessment of the stress and strain fields inside the isolators. The effect of shape factor has a central position in both experimental and numerical investigations.

EFFECT OF SHAPE FACTOR ON THE MECHANICAL PROFILES OF SQUARE U-FREI

For a square isolator with side dimension *a*nd thickness of an elastomer layer t_e, the shape factor is given by /23/

$$S=\frac{a}{4t_e}. \tag{1}$$

Vertical stiffness (K_V) of a laminated elastomeric isolator is

$$K_V=\frac{E_c A}{t_r}, \tag{2}$$

where: E_c is the compression modulus; A is the full cross-sectional area of the isolator.

According to Kelly and Konstantinidis /24/, the compression modulus, E_c, for a rectangular isolator having the width of $2b$ and length l, can be expressed in terms of the shape factor, S, the aspect ratio of isolator, $\rho = 2b/l$, and the shear modulus, G, as

$$E_c=\frac{384}{\pi^4}GS^2(1+\rho)^2\sum_{m=1,3,5,\ldots}^{\infty}\frac{1}{m^4}\left(1-\frac{2\rho}{m\pi}\tanh\left(\frac{m\pi}{2\rho}\right)\right). \tag{3}$$

In particular, the compression modulus for a square isolator is $E_c = 6.748GS^2$. Thus, the vertical stiffness of a square isolator is given by the formula

$$K_V=\frac{6.748GS^2A}{t_r}. \tag{4}$$

The effective bending stiffness $(EI)_{eff}$ for a rectangular isolator can be expressed as

$$(EI)_{eff}=\frac{72GIS^2}{\pi^4}(1+\rho)^2\sum_{n=1}^{\infty}\frac{1}{n^4}\left(1-\frac{2\rho}{n\pi}\tanh\left(\frac{n\pi}{2\rho}\right)\right), \tag{5}$$

where: I is the moment of inertia, given by

$$I=\frac{l(2b)^3}{12}=\frac{2lb^3}{3}. \tag{6}$$

The effective bending stiffness for a square isolator is

$$(EI)_{eff}=2.228GIS^2. \tag{7}$$

It can be seen from Eqs.(4) and (7), the values of the vertical stiffness and effective bending stiffness of a U-FREI is directly proportional to the square of shape factor.

However, the horizontal response of U-FREI is relatively complex. Deformed shapes of conventional FREIs and unbonded FREIs under a given horizontal displacement are compared in Fig. 1. According to /18/, the reduction of horizontal stiffness of U-FREI with increasing horizontal displacement depends on the contact area between the isolator and the support surfaces, or rollover deformation and shear modulus. The effective horizontal stiffness of U-FREI is expressed as

$$K_h=\frac{G_{eff}A_{eff}}{t_r}, \tag{8}$$

where: G_{eff} and A_{eff} are the effective shear modulus and the effective plan area in contact with the support surfaces of the U-FREI, respectively.

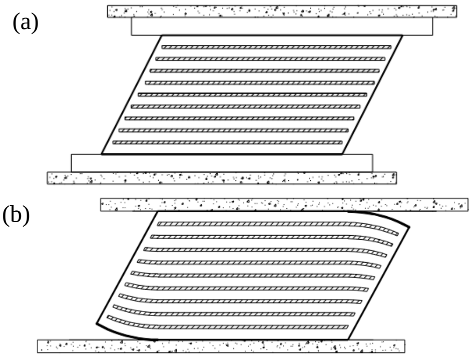

Figure 1. Deformed shapes of different types of isolators under horizontal displacement: a) conventional isolator; b) U-FREI.

For square U-FREIs with identical material properties, thickness of elastomer as well as reinforcement layers and total height, but different sizes of plan dimensions (or different shape factors), the horizontal response is dependent on the contact area of the isolator with the support surfaces or the shape factor. Thus, the effect of shape factor on horizontal response of prototype square U-FREIs is important and therefore determines the design, production and in-field application of prototype isolators.

EXPERIMENTAL STUDY

Experimental setup

The design of the prototype U-FREIs that are considered in this study is based on their application for seismic isolation of a two-story masonry building which is under construction at Tawang, India (Fig. 2). The building is the first such U-FREIs supported prototype masonry building constructed anywhere in the world. Vulcanized elastomer layers and bi-directional (0°/90°) carbon fiber fabric are used for the construction of these isolators, with the support of METCO Pvt.

Ltd., Kolkata, India. Total four prototype U-FREIs with two different sizes in plane including two specimens of size 250×250×100 mm (noted as type A with names of A(1,2)) and two specimens of size 310×310×100 mm (noted as type B with names of B(1,2)) are considered in this study. These isolators are made from eighteen elastomer layers interleaved and bonded with seventeen layers of carbon fiber reinforcement sheets (Fig. 3). The tests of all the specimens have been made at Structural Engineering Laboratory, Indian Institute of Technology Guwahati, India, under the application of horizontal varying cyclic displacement and constant vertical pressure equal to $p \approx 5.6$ MPa simultaneously. More details about the experimental setup, the shape factor and composition of the isolators as well as the loading displacement history can be found in Ngo et al. /18-19, 25/. The experimental test setup and the application of cyclic displacement are shown in Figs. 4-5, respectively. The geometrical details and material properties of the isolators are shown in Table 1.

Figure 2. Prototype base-isolated masonry building located at Tawang, India.

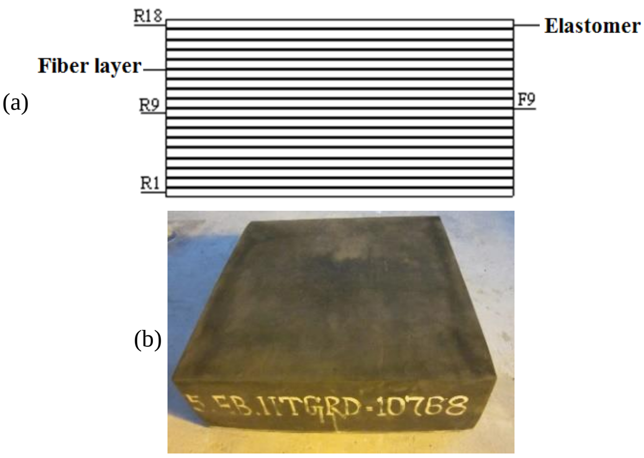

Figure 3. Details of prototype U-FREI: a) schematic representation of elastomer and fiber layers; b) 3D view.

Figure 4. Actual experimental setup for the evaluations of horizontal stiffness of U-FREIs.

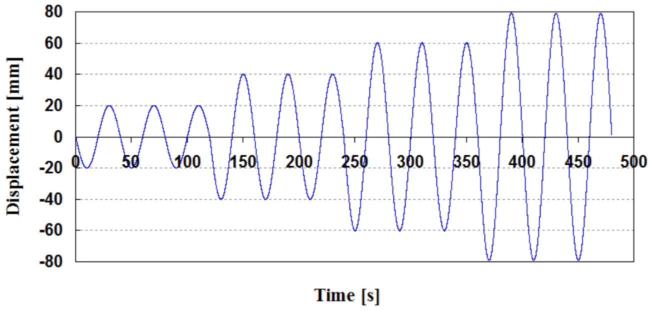

Figure 5. Applied horizontal displacement time history.

Table 1. Geometry and material properties of square isolators.

Description	Isolator type *A*	Isolator type *B*
Number of isolators, *N*	2 - $A_{(1,2)}$	2 - $B_{(1,2)}$
Number of elastomer layer, n_e	18	18
Thickness of single elastomer layer, t_e (mm)	5.0	5.0
Total height of elastomer, t_r (mm)	90	90
Number of carbon fiber layer, n_f	17	17
Thickness of single fiber layer, t_f (mm)	0.55	0.55
Shape factor, *S*	12.5	15.5
Shear modulus of elastomer, *G* (MPa)	0.90	0.90
Elastic modulus of carbon fiber laminate, *E* (GPa)	40	40
Poisson’s ratio of carbon fiber laminate, μ	0.20	0.20

Experimental results

Deformed shapes: In Fig. 6 the deformed shape of a typical specimen as obtained from the experimental tests at 80 mm amplitude of horizontal displacement is shown. It is observed that part of the top and bottom surfaces of U-FREI lose contact with the supports as a result of stable rollover response without any damage. This reduction in contact area leads to decrease in the effective horizontal stiffness of the isolators and results in nonlinear behaviour of the elastomers due to large displacements.

Figure 6. Experimentally observed deformed shape of a typical U-FREI at applied horizontal displacement of 80 mm.

Hysteresis loops: During the experiments, the horizontal displacements are measured by Linear Variable Differential Transformers (LVDTs) and the shear forces are measured by load cells. Both LVDTs and load cells are mounted in the servo-hydraulic actuator. Since the shear force measurements represent the total shear force that is applied to two specimens simultaneously, it is divided by two in order to obtain the shear force per specimen in an average sense. As a result, the hysteresis loops of the specimens are obtained which show the relationship between the shear force and cyclic horizontal displacement. Some representative hysteresis loops obtained in this study are shown in Fig. 7.

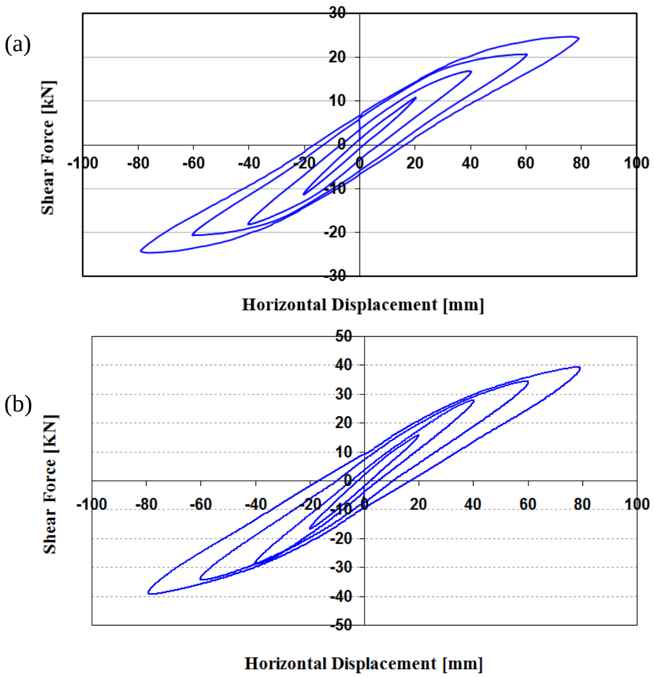

Figure 7. Hysteresis loops for U-FREI specimens from experimentally observed data: a) $A_{(1,2)}$; b) $B_{(1,2)}$.

Stiffness and damping: Among the most important response quantities of the U-FREIs (and the seismic isolators in general) that determine the seismic response of the structures in which they are installed, are the effective horizontal stiffness and the equivalent viscous damping (or effective damping factor). These mechanical properties are calculated based on the hysteresis loops. According to ASCE 7 /26/, the effective horizontal stiffness of an isolator at any amplitude of horizontal displacement is defined as

$$K_{eff}^{h}=\frac{F_{\max}-F_{\min}}{u_{\max}-u_{\min}}, \tag{9}$$

where: F_{max}, F_{min} are maximum and minimum values of the shear force; u_{max}, u_{min} are maximum and minimum values of the horizontal displacement.

The equivalent viscous damping factor of an isolator (β) depends mainly on the energy dissipated in each cycle (W_d), which is equal to the area enclosed by the hysteresis loop. The damping factor β is computed as follows

$$\beta=\frac{W_d}{2\pi K_{eff}^{h}\Delta_{\max}^{2}}, \tag{10}$$

where: $\Delta_{\max}$ is the average of the positive and negative maximum displacements; $\Delta_{\max} = (|u_{\max}| + |u_{\min}|)/2$.

The aforementioned mechanical properties depend not only on the amplitude of the horizontal displacement, but also on the response history. For this reason, for a specific value of horizontal displacement amplitude, they are estimated as an average value taken over three consecutive loading cycles of the U-FREIs with this amplitude. The estimated values are shown in Table 2.

Table 2. Properties of U-FREIs from experimental tests.

Amplitude (mm)	u/t_r	$A_{(1,2)}$		$B_{(1,2)}$	
		K_{eff}^{h} (kN/m)	β (%)	K_{eff}^{h} (kN/m)	β (%)
20	0.22	507.26	5.00	814.54	5.82
40	0.44	410.21	9.67	708.04	6.89
60	0.67	339.01	12.83	573.36	10.14
80	0.89	318.68	12.07	497.48	11.84

It is obvious in Table 2 that as the horizontal displacement amplitude increases, the effective stiffness and the equivalent viscous damping factor of the U-FREIs decreases and increases, respectively. The decrease in the effective stiffness ranges from 37.2 to 43.2 % for specimens $A_{(1,2)}$ and $B_{(1,2)}$. It is obvious that the decrease in the effective horizontal stiffness that comes from the rollover deformation leads to a substantial increase in the eigenperiod of the base isolated structure which in turn increases the seismic response control efficiency of the isolators.

FINITE ELEMENT ANALYSIS

Finite Element (FE) simulations of U-FREIs under simultaneous action of constant vertical pressure and cyclic horizontal displacement are carried out using ANSYS v.14.0 /27/. Initially, an assessment of the accuracy of the FE analysis is made by simulating the experiments and comparing the numerical and the experimental results. Afterwards, the dynamic behaviour of the seismic isolators is evaluated at horizontal displacement amplitude larger than that imposed during the experiments (1.50t_r vs 0.89t_r, where t_r is the total height of elastomer). Experimental testing under such high amplitudes is not possible due to practical limitations, and therefore, the numerical simulation is the only way to predict the response of the isolators under these circumstances. The loading protocol considered in the FE analysis is similar to that considered in the experimental study.

Description of the FE model

The elastomer is modelled using the SOLID185 element in ANSYS, which is a structural solid element having 8 nodes with three Degrees of Freedom (DOFs) each, i.e. translation in the global x, y, and z directions. This element can simulate a variety of nonlinear constitutive material models, including plasticity, hyper-elasticity, stress stiffening and creep. Geometrical nonlinearities due to large deformation and strain can be accommodated. Furthermore, the SOLID 185 element is capable of simulating the deformation of nearly incompressible elastoplastic materials and of fully incompressible hyper-elastic materials through a mixed u-P formulation based on Lagrange multipliers. The element

SOLID46 is used for modelling the fiber reinforcement layers. This is a 3-D 8-node layered structural solid designed to model layered thick shells or solids. Bi-directional (0°/ 90°) layers have been used for modelling the fiber-reinforcement which are bonded between elastomer layers.

At the top and bottom of the isolator, two rigid horizontal plates are defined to simulate the superstructure and substructure. These plates are also modelled using SOLID185, and contact elements are used for simulating their contact with the isolator. More specifically, surface-to-surface contact elements CONTA173 are used to define the top and bottom surfaces of the elastomer, and target elements TARGE170 are used to define the interior surface of the corresponding rigid plates. At the interface between the contact and target surfaces, a maximum Coulomb friction coefficient equal to 0.85 is used to avoid sliding. The specification of this coefficient has been made based on experimental data and the literature. The friction coefficient between rubber and dry concrete ranges between 0.60 and 0.85 (or even higher in some cases). However, a larger value equal to 1.0 has been selected in FE simulations, /28-29/.

Mesh generation is carried out with a hexagonal volume sweep algorithm. Figure 8 shows the FE mesh of isolator type A and selected axes. Fibers are oriented parallel to *x*-axis at their 0° direction and parallel to *y*-axis at their 90° direction. An earlier mesh sensitivity study is performed for the selection of the mesh size to ensure normal convergence.

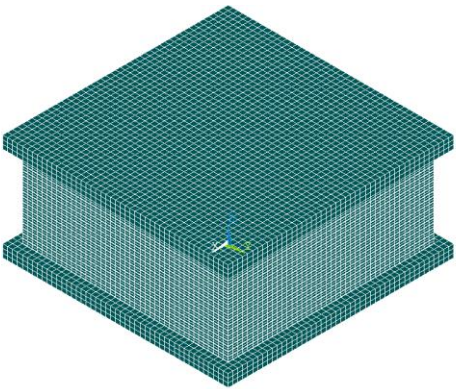

Figure 8. Adopted finite element mesh for U-FREI type *A*.

Regarding the boundary conditions, the bottom plate is fixed, whereas vertical pressure equal to 5.6 MPa and cyclic horizontal displacement is applied at the top plate. Three complete sinusoidal cycles with increasing displacement amplitude up to 1.50t_r (135 mm) are applied on the top steel plate, as shown in Fig. 5.

Material model

The constitutive properties of the material models used in the FE analysis are shown in Table 1. A hyper-elastic material model with time dependent viscoelasticity is used for the elastomer. Such material models involve large and recoverable elastic strains and their stiffness varies depending on the stress level, according to a given strain energy potential. This behaviour is characteristic of rubber-like and other polymer materials. Hyperelasticity is implemented through the Ogden three-term model, which is characterized by shear (G_e) and bulk (k_e) modulus of the elastomer. Also, the visco-elastic shear response behaviour is modelled by Prony series parameters. The following values are used for the material model in this study, /30/:

Ogden (three-term): μ_1 = 1.89×10^6 N/m^2; μ_2 = 3600 N/m^2; μ_3 = -30000 N/m^2; α_1 = 1.3; α_2 = 5; α_3 = -2;

Prony shear response: a_1 = 0.3333; t_1 = 0.04; a_2 = 0.3333; t_2 = 100.

FE analysis results

Validation of FE model of U-FREIs: Figure 9 shows the deformation of the U-FREI for amplitude of horizontal displacement equal to 80 mm, as obtained from the FE analysis results. It is obvious that the deformed geometry of the isolator resembles very much to that of the experiment, shown in Fig. 6, in terms of both the roll-off between the faces of the isolator and the contact supports, and also the general deformation pattern.

In order to get the total shear force experienced by the isolator, the horizontal reaction forces at the nodes, where the displacement is imposed, are summed. Based on this, the hysteresis loop of each isolator has been calculated, as shown in Fig. 10. Also, the corresponding experimental data are plotted in the same figure for comparison, for displacement up to 80 mm. It is apparent that there is a very good agreement between the numerical and the experimental curves.

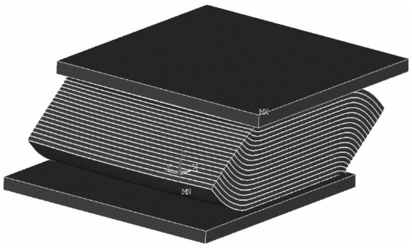

Figure 9. Deformed shape of typical U-FREI at 80 mm horizontal displacement, obtained from FE analysis.

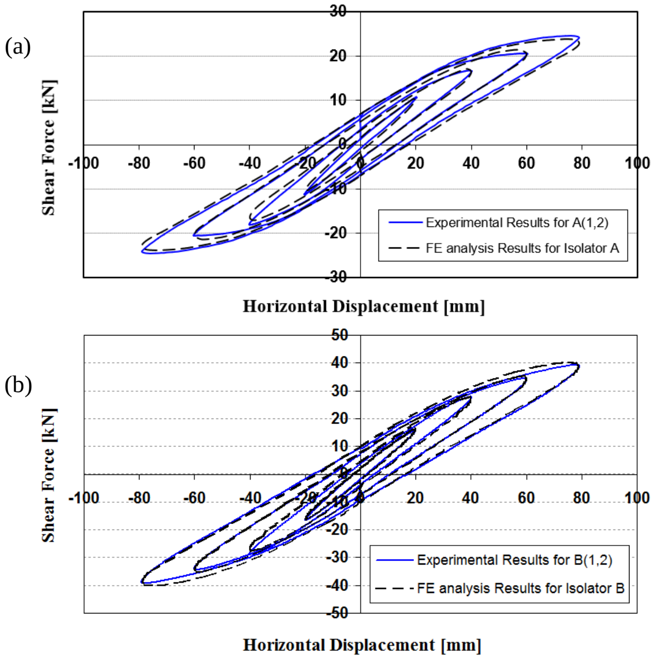

Figure 10. Comparison of hysteresis loops of different U-FREIs, obtained from experiment and FE analysis: a) type *A*; b) type *B*.

Mechanical properties of the U-FREIs: Table 3 presents the effective horizontal stiffness and the equivalent viscous damping obtained from FE analysis. These are calculated from Eqs.(9) and (10). It is seen from Table 3 that the effective horizontal stiffness of U-FREIs decreases as the horizontal displacement increases. Furthermore, according to Tables 2 and 3, there is reasonable agreement between FE results and experimental data in terms of the mechanical properties of the U-FREIs for displacements ranging from 20 to 80 mm. Based on this observation, it is assumed that FE analysis results will be reasonably accurate for larger displacements (up to 135 mm).

Table 3. Properties of U-FREIs, obtained from FE analysis.

Amplitude (mm)	u/t_r	U-FREI type *A*		U-FREI type *B*	
		K_{eff}^h (kN/m)	β (%)	K_{eff}^h (kN/m)	β (%)
20.0	0.22	515.87	7.58	814.23	6.86
40.0	0.44	426.93	9.60	688.00	8.52
60.0	0.67	357.01	12.05	586.30	10.35
80.0	0.89	301.67	13.46	508.60	12.16
90.0	1.00	281.34	14.11	480.09	12.57
112.5	1.25	247.09	14.58	433.13	13.08
135.0	1.50	222.03	15.42	401.33	13.68

EFFECT OF SHAPE FACTOR ON THE HORIZONTAL RESPONSE OF SQUARE U-FREI

U-FREI types *A* and *B* have same component layers and total height of 100 mm, same shear modulus of elastomer of 0.90 MPa. They are subjected to same vertical pressure of p = 5.6 MPa and cyclic horizontal displacement up to $1.50t_r$. However, they are only different in size of plan area or shape factor, *S*. The values of shape factor are 12.5 for U-FREI type *A*, and 15.5 for U-FREI type *B*. Effective horizontal stiffness, stress in elastomer, and fiber reinforcement layers of U-FREI types *A* and *B* are compared to appreciate the influence of shape factor.

Effective horizontal stiffness of U-FREIs

It may be seen from Tables 2 and 3 that the effective horizontal stiffness of U-FREI type *A* (*S* = 12.5) is smaller than the corresponding value of U-FREI type *B* (*S* = 15.5) at any given applied displacement due to the smaller contact area of isolator with the support surfaces. Further, the effective horizontal stiffness decreases with increasing horizontal displacement of U-FREIs due to rollover deformation. Figure 11 shows the variation of the effective horizontal stiffness of U-FREI types *A* and *B* as the displacement increases. Results from both experiments and FE analyses are plotted. It may be observed from FE analysis results that the rates of decrease in horizontal stiffness of isolator *A* (*S* = 12.5) and isolator *B* (*S* = 15.5) are found to be 57.0 and 50.7 %, in respect, as the applied displacement varies from 20 to 135 mm.

Stress in elastomer layers

It is considered that the horizontal displacement is imposed on the isolators along the global *x*-axis. The stress tensor is given in terms of the global *x*, *y* and *z*-axes. Due to the symmetry of the problem, FE analysis results show similar values for stresses S_{11} and S_{22}, and thus, only S_{11} and S_{33} are plotted.

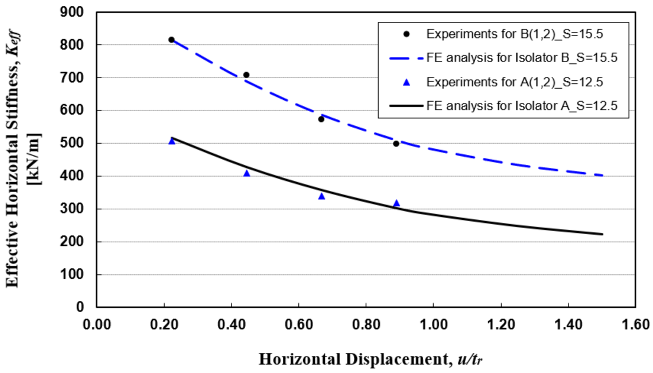

Figure 11. Effective horizontal stiffness vs. displacement of U-FREI types *A* and *B*.

Contours of normal stresses S_{11} and S_{33} in elastomer layers of a half U-FREI corresponding to maximum applied displacement of 135 mm ($u = 1.50t_r$) are shown in Figs. 12 and 13. For better illustration of the results, these contours are plotted only for the one half of the model. While the isolator displaces horizontally, compression is observed near the centre of the isolator. In addition, tension develops inside the U-FREI, near the area where no contact occurs with the rigid plates, while other regions remain under compression. However, this tensile stress is not transmitted to the isolator's contact support, due to its rollover response. The unbalanced moments are resisted by the offset between the two resultants of the vertical loads coming from the top and bottom surfaces.

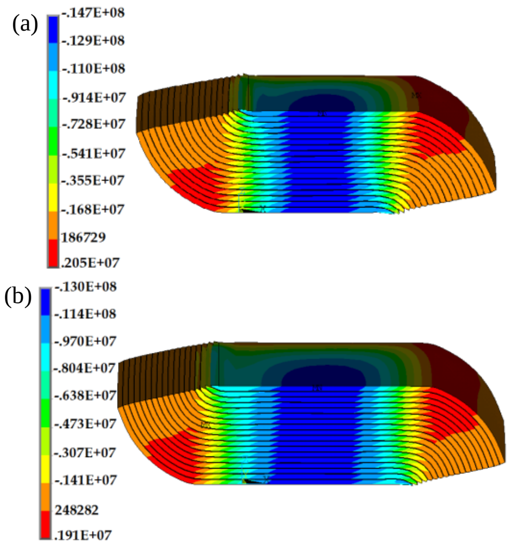

Figure 12. Contour of normal stress S_{11} (N/m^2) in elastomer layers of a half isolator at horizontal displacement of 135 mm (positive value indicates tension): a) U-FREI type *A*; b) U-FREI type *B*.

In comparison of U-FREI types *A* and *B*, the area of compression region in U-FREI type *A* (*S* = 12.5) is smaller than that in U-FREI type *B* (*S* = 15.5) due to the area in contact with support surfaces of isolators. It may however be noted that the applied vertical pressure, material properties and the thickness of a single elastomer layer are same for both these square U-FREIs. Lower value of shape factor of U-FREI leads to lower value of area in contact with support surfaces of the isolator, and also leads to lower value of effective horizontal stiffness of the isolator.

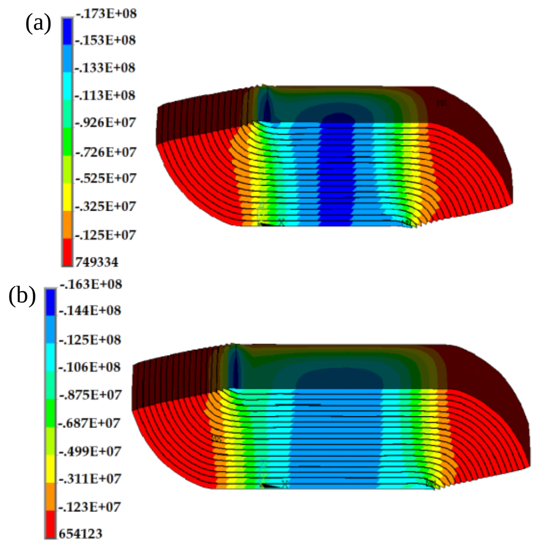

Figure 13. Contour of normal stress S_{33} (N/m^2) in elastomer layers of a half isolator at horizontal displacement of 135 mm (positive value indicates tension): a) U-FREI type *A*; b) U-FREI type *B*.

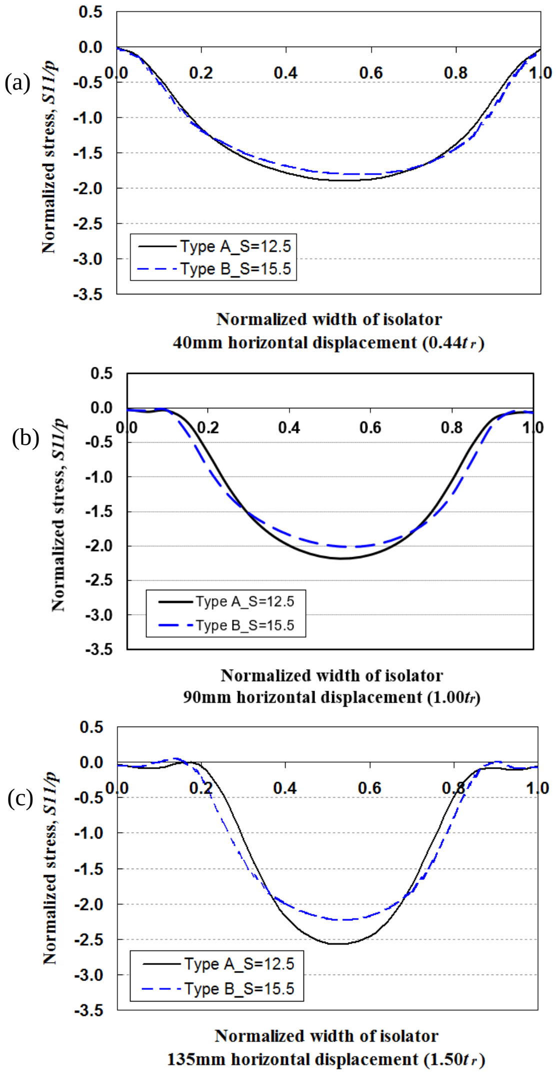

Figure 14. Comparison of normalized stress S_{11}/p plotted along the width in elastomer layer at mid-height of U-FREI types A and B at different horiz. displacements: a) $u = 0.44t_r$; b) $u = 1.00t_r$; c) $u = 1.50t_r$.

Figures 14 and 15 represent the comparison of normalized stresses S_{11}/p and S_{33}/p plotted along the width of the 9-th elastomer layer, located adjacent to the mid-height of U-FREI types A and B at different horizontal displacements. It can be seen from Figs. 14 and 15 that peak values of compressive stress of U-FREI type A (S = 12.5) are higher than those of U-FREI type B (S = 15.5) at any given displacement, while the length of compression region of isolator A is smaller than that of isolator B. Specifically, at $u = 1.50t_r$, the peak values of normalized compressive stresses S_{11}/p and S_{33}/p of U-FREI type A are found to be 15.1 and 14.5 % higher than corresponding values of U-FREI type B.

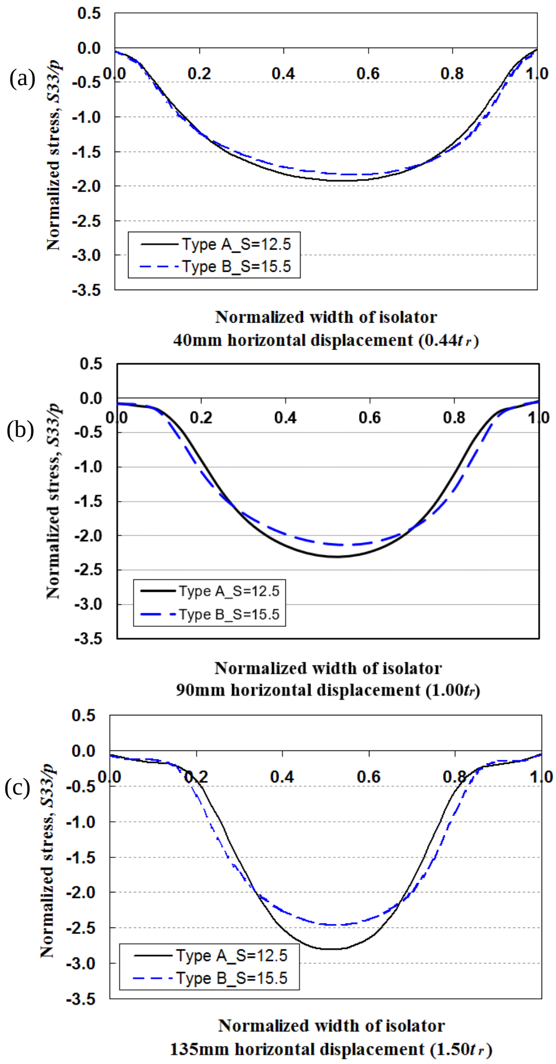

Figure 15. Comparison of normalized stress S_{33}/p plotted along the width in the elastomer layer at mid-height of U-FREI types *A* and *B* at different horiz. displacements: a) $u = 0.44t_r$; b) $u = 1.00t_r$; c) $u = 1.50t_r$.

Comparison of shear strain plotted along the width of the 9-th elastomer layer, located adjacent to the mid-height of U-FREI types *A* and *B*, at different horizontal displacements is shown in Fig. 16. According to Fig. 16, the peak values of shear strain of U-FREI types *A* and *B* at any given displacement are quite comparable, while the uniform region of shear strain of isolator *B* (S = 15.5) is larger than that of isolator *A* (S = 12.5) due to the larger length of the region in contact with the top and bottom supports.

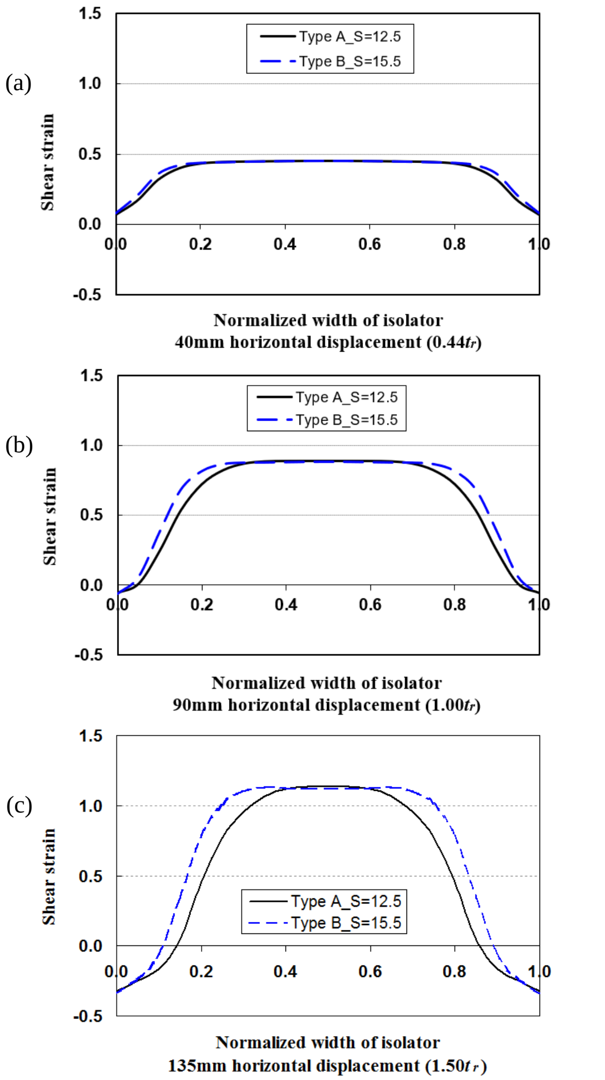

Figure 16. Comparison of shear strain plotted along the width in elastomer layer at mid-height of U-FREI types A and B at different horizontal displacements: a) $u = 0.44t_r$; b) $u = 1.00t_r$; c) $u = 1.50t_r$.

Stress in fiber reinforcement layer

Comparison of normalized stress S_{11}/p plotted along the width of the 9-th fiber reinforcement layer, located to the mid-height of U-FREI types *A* and *B* at different horizontal displacements is shown in Fig. 17. Similar to the comparison of compressive stress in mid elastomer layer of U-FREI in Fig. 17, the peak value of normalized tensile stress S_{11}/p of U-FREI type *A* (S = 12.5) is higher than that of U-FREI type *B* (S = 15.5) at a given displacement. Specifically, at $u = 1.50t_r$ the peak value of tensile stress S_{11}/p of U-FREI type *A* is found to be 15.4 % higher than that of U-FREI type *B*.

CONCLUSIONS

In this study the response of prototype U-FREIs under horizontal cyclic excitation is studied both experimentally and numerically. After checking that the FE models developed are verified by the corresponding experiments, the effect of the shape factor on the dynamic behaviour of square U-FREIs is considered. The concluding remarks are as follows:

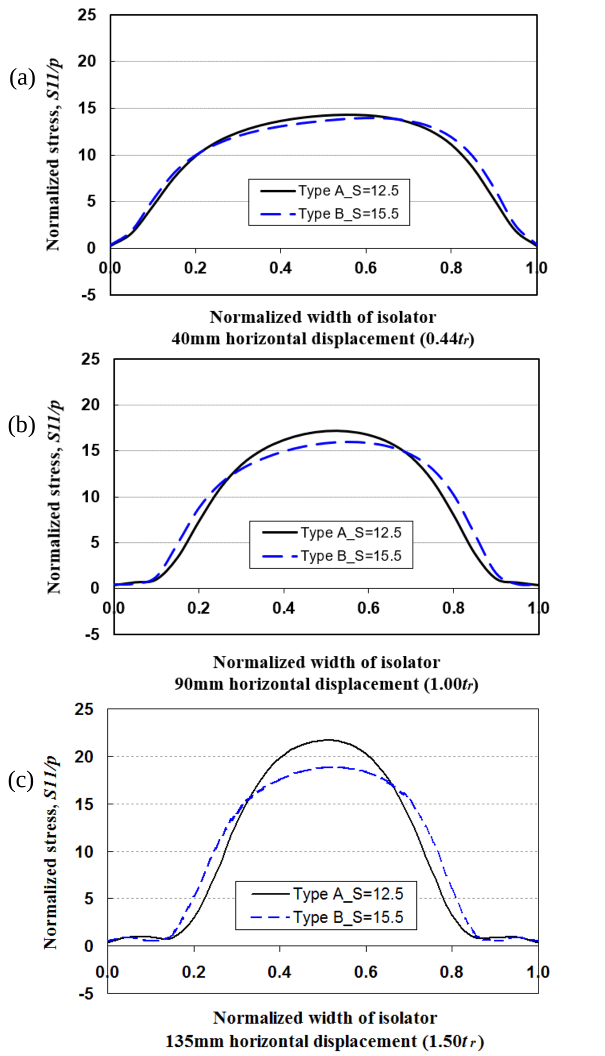

Figure 17. Comparison of normalized stress S_{11}/p plotted along the width in fiber layer at mid-height of U-FREI types *A* and *B* at different horizontal displacements: a) $u = 0.44t_r$; b) $u = 1.00t_r$; c) $u = 1.50t_r$.

- As the horizontal displacement of a U-FREI increases, its effective horizontal stiffness decreases and its equivalent viscous damping increases, due to the presence of rollover deformation.
- The experimental and FE analysis results are in reasonable agreement for horizontal displacements up to 80 mm. FE analysis can be adopted effectively to a very large range of displacement (80 to 135 mm), which may be otherwise difficult in experimental study.
- Effective horizontal stiffness of U-FREI with smaller shape factor is smaller than the corresponding value of U-FREI with larger shape factor at any given applied displacement due to the smaller area of contact between the isolator and the support surfaces.
- The maximum compressive stresses in elastomer layers of the U-FREI with smaller shape factor are higher than those of U-FREI with larger shape factor, while the maximum shear strains in elastomer layers of these U-FREIs are quite comparable at any given applied displacement.
- The maximum tensile stresses in fiber layers of U-FREI with smaller shape factor are higher than those of U-FREI with larger shape factor at any given applied displacement.

REFERENCES

1. Luo, J., Fahnestock, L.A., LaFave, J.M. (2017), *Nonlinear static pushover and eigenvalue modal analyses of quasi-isolated highway bridges with seat-type abutments*, Structures, 12: 145-167. doi: 10.1016/j.istruc.2017.08.006
2. Shiravand, M.R., Rasouli, M. (2019), *Effects of substructure mass participation on natural period of multi-column base isolated bridges*, Structures, 20: 88-104. doi: 10.1016/j.istruc.2019.03.002
3. Shoaei, P., Mahsuli, M. (2019), *Reliability-based design of steel moment frame structures isolated by lead-rubber bearing systems*, Structures, 20: 765-778. doi: 10.1016/j.istruc.2019.06.020
4. Kelly, J.M. (1999), *Analysis of fibre-reinforced elastomeric isolators*, J Seismol. Earthquake Eng. 2(1): 19-34.
5. Kelly, J.M., Takhirov, S.M., Analytical and experimental study of fiber-reinforced elastomeric isolator, PEER Report, Pacific Earthquake Eng. Research Center, University of California, Berkeley, USA, 2001/11.
6. Kelly, J.M., Takhirov, S.M., Analytical and experimental study of fiber-reinforced strip isolators, PEER Report, Pacific Earthq. Eng. Res. Center, Univ. of California, Berkeley, USA, 2002/11.
7. Moon, B.Y., Kang, G.J., Kang, B.S., Kelly, J.M. (2002), *Design and manufacturing of fiber reinforced elastomeric isolator for seismic isolation*, J Mater. Proc. Technol. 130-131: 145-150. doi: 10.1016/S0924-0136(02)00713-6
8. Toopchi-Nezhad, H., Tait, M.J., Drysdale, R.G. (2008), *Testing and modeling of square carbon fiber-reinforced elastomeric seismic isolators*, Struct. Control Health Monit. 15(6): 876-900. doi: 10.1002/stc.225
9. Toopchi-Nezhad, H., Tait, M.J., Drysdale, R.G. (2008), *Lateral response evaluation of fiber-reinforced neoprene seismic isolator utilized in an unbonded application*, J Struct. Eng. 134(10): 1627-1637. doi: 10.1061/(ASCE)0733-9445(2008)134:10(1627)
10. Toopchi-Nezhad, H., Drysdale, R.G., Tait, M.J. (2009), *Parametric study on the response of stable unbonded-fiber reinforced elastomeric isolators (SU-FREIs)*, J Compos. Mater. 43(15): 1569-1587. doi: 10.1177 /0021998308106322
11. Russo, G., Pauletta, M. (2013), *Sliding instability of fiber-reinforced elastomeric isolators in unbonded applications*, Eng. Struct. 48: 70-80. doi: 10.1016/j.engstruct.2012.08.031
12. Spizzuoco, M., Calabrese, A., Serino, G. (2014), *Innovative low-cost recycled rubber-fiber reinforced isolator: Experimental test and Finite Element Analyses*, Eng. Struct. 76(1): 99-111, doi: 10.1016/j.engstruct.2014.07.001
13. Strauss, A., et al. (2014), *Experimental investigations of fiber and steel reinforced elastomeric bearings: Shear modulus and damping coefficient*, Eng. Struct. 75(15): 402-413. doi: 10.1016 /j.engstruct.2014.06.008
14. Dezfuli, F.H., Alam, M.S. (2014), *Performance of carbon fiber-reinforced elastomeric isolators manufactured in a simplified process: experimental investigations*, Struct. Cont. Health Monit. 21(11): 1347-1359. doi: 10.1002/stc.1653
15. Van Engelen, N.C., Osgooei, P.M., Tait, M.J., Konstantinidis, D. (2014), *Experimental and finite element study on the compression properties of Modified Rectangular Fiber-Reinforced Elastomeric Isolators (MR-FREIs)*, Eng. Struct. 74(1): 52-64. doi: 10.1016/j.engstruct.2014.04.046
16. Toopchi-Nezhad, H. (2014), *Horizontal stiffness solutions for unbonded fiber reinforced elastomeric bearings*, Struct. Eng. Mech. 49(3): 395-410. doi: 10.12989/sem.2014.49.3.395
17. Das, A., Dutta, A., Deb, S.K. (2015), *Performance of fiber-reinforced elastomeric base isolators under cyclic excitation*, Struct. Cont. Health Monit. 22(2): 197-220, doi: 10.1002/stc.1668
18. Ngo, V.T., Dutta, A., Deb, S.K. (2017), *Evaluation of horizontal stiffness of fibre-reinforced elastomeric isolators*, Earthquake Eng. Struct. Dyn. 46(11): 1747-1767. doi: 10.1002/eqe.2879
19. Ngo, V.T. (2018), *Effect of shear modulus on the performance of prototype un-bonded fiber reinforced elastomeric isolators*, J Sci. Technol. Civil Eng. 12(5): 10-19. doi: 10.31814/stce.nuce2018-12(5)-02
20. Ngo, V.T., Deb, S.K., Dutta, A. (2018), *Effect of horizontal loading direction on performance of prototype square unbonded fibre reinforced elastomeric isolator*, Struct. Cont. Health Monit. 25(9). doi: 10.1002/stc.2112
21. Losanno, D., Spizzuoco, M., Calabrese, A. (2019), *Bidirectional shaking-table tests of unbonded recycled-rubber fiber-reinforced bearings (RR-FRBs)*, Struct. Cont. Health Monit. 26(9). doi: 10.1002/stc.2386
22. Calabrese, A., et al. (2019), *Recycled rubber fiber-reinforced bearings (RR-FRBs) as base isolators for residential buildings in developing countries: The demonstration building of Pasir Badak, Indonesia*, Eng. Struct. 192: 126-144. doi: 10.1016/j.engstruct.2019.04.076
23. Naeim, F., Kelly, J.M., Design of Seismic Isolated Structures: From Theory to Practice, John Wiley & Sons, New York, USA, 1999.
24. Kelly, J.M., Konstantinidis, D.A., Mechanics of Rubber Bearings for Seismic and Vibration Isolation, John Wiley & Sons, Ltd, 2011. doi: 10.1002/9781119971870
25. Ngo, V.T., Dutta, A., Deb, S.K. (2020), *Predicting stability of a prototype unbonded fiber-reinforced elastomeric isolator by finite element analysis*, Int. J Comp. Methods, 17(10). doi: 10.1142/S0219876220500152
26. ASCE/SEI 7-10, Minimum Design Loads for Buildings and Other Structures, American Society of Civil Engineers, Reston, Virginia, USA, 2013. doi: 10.1061/9780784412916
27. ANSYS version 14.0, Help System, Analysis Guide, ANSYS, Inc, USA, 2014
28. Toopchi-Nezhad, H., Tait, M.J., Drysdale, R.G. (2011), *Bonded versus unbonded strip fiber reinforced elastomeric isolators: Finite element analysis*, Compos. Struct. 93(2): 850-859. doi: 10.1016/j.compstruct.2010.07.009
29. Konstantinidis, D., Moghadam, S.R. (2016), *Compression of unbonded rubber layers taking into account bulk compressibility and contact slip at the supports*, Int. J Solid Struct. 87(C): 206-221. doi: 10.1016/j.ijsolstr.2016.02.008
30. Holzapfel, G.A. (1996), *On large strain viscoelasticity: Continuum formulation and finite element applications to elastomeric structures*, Int. J Numer. Methods Eng. 39(22) 3903-3926. doi: 10.1002/(SICI)1097-0207(19961130)39:22<3903::AID-NME34>3.0.CO;2-C